J. Phys. B: At. Mol. Opt. Phys. **32** (1999) 1097–1112. Printed in the UK PII: S0953-4075(99)97214-0

Electron impact double ionization of C^- and O^- ions

C Bélenger, D S Belic†, D J Yu‡ and P Defrance

Université Catholique de Louvain, Département de Physique 2, chemin du Cyclotron, B-1348 Louvain-la-Neuve, Belgium

Received 7 September 1998

Abstract. Absolute cross section measurements for double ionization of C^- and O^- ions by electron impact are reported. The animated crossed beams method has been employed in the energy range from ionization threshold to approximately 2.5 keV. Present results are found to be smaller than the experimental result of Steidl *et al* (1995 *Proc. 19th Int. Conf. Physics of Electronic and Atomic Collisions (Whistler)* ed J B A Mitchell *et al* p 564). The role of slow positive ions trapped in the electron beam could explain the observed discrepancy. The study of double ionization processes along the fluorine isoelectronic sequence (for O^-, Ne^+ and Ar^{9+} ions) shows that the results for multiply charged ions are strongly lower than predicted by classical scaling. A systematic threshold energy shift is observed in the sequence and, for O^-, the position of the cross section maximum is found to be at an unusually high energy. The autoionizing 1P state belonging to the ($1s^2 2s2p^5$) configuration of atomic oxygen is clearly seen to contribute to the O^+ signal above 23.7 eV. Other autoionizing states are also seen to play a role around the K-shell ionization threshold. The Bethe-plot of present data shows that the high energy behaviour of cross sections is dominated by the E^{-1}, term for C^-, while it is dominated by the logarithmic term for O^-.

1. Introduction

Various processes can contribute to electron impact double ionization (DI), depending on the incident electron energy and structure of the parent and intermediate atomic or ionic states. In addition to direct double ionization (DDI) of outer-shell electrons, indirect processes can contribute as well. The most important of them is ionization–autoionization (IA) which appears if autoionization follows ejection of one inner-shell electron. For a review of indirect ionization processes, see for instance Moores and Reed (1994).

DI of negative atomic ions by electron impact was first investigated experimentally for hydrogen (Yu *et al* 1992). That measurement showed that, as expected from the ion structure, only DDI plays a role in the reaction. This situation is very different from the one encountered for various atoms or positive ions where experiment and theory have frequently demonstrated the major contribution of indirect mechanisms to double electron ejection. This situation holds in particular for multiply-charged ions on which most of the recent measurements were focused.

DI has also been investigated experimentally for the negative carbon, oxygen and fluorine ions. Results were first obtained for C^- and O^- in our laboratory (Defrance *et al* 1993). General trends of cross sections were drawn, but experimental difficulties prevent one from observing the cross section either in the low energy region or in the high one. Those results are

† Present address: Faculty of Physics, PO Box 550, 11000 Beograd, Yugoslavia.

‡ Present address: Centre of Space Science and Applied Research, Chinese Academy of Sciences, PO Box 8701, Beijing 100080, People's Republic of China.

0953-4075/99/051097+16$19.50

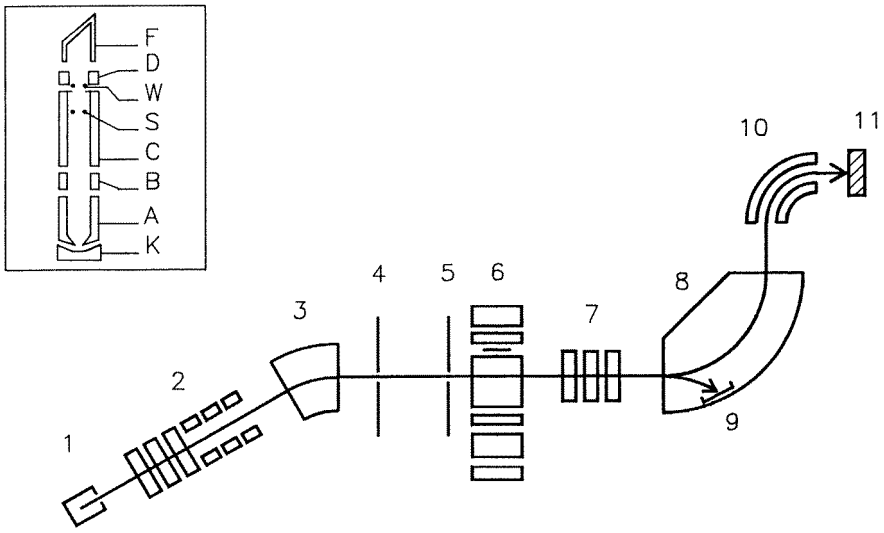

Figure 1. Schematic diagram of the apparatus: (1), Colutron ion source; (2), electrostatic lenses; (3), magnetic mass selector; (4, 5), diaphragms; (6), electron gun; (7), electrostatic lens; (8), magnetic analyser; (9), Faraday cup; (10), spherical electrostatic deflector; (11), detector. The inset shows a schematic plan of the electron gun; (K), cathode; (A), anode; (B), focusing and deflecting electrodes; (C), final electrodes; (S), wires for the sweeping speed measurement; (W), wires; (D), suppressors; (F), Faraday cup.

considered as preliminary ones. Experimental results have also been obtained at the Giessen University for C^-, O^- and F^- (Steidl *et al* 1995).

Present results have been obtained with the same apparatus as before. Minor modifications were made in order to overcome the above-mentioned difficulties. Data cover the energy range from threshold to 2.5 keV. Particular attention is paid to identify possible contributions from various indirect DI processes.

From the theoretical point of view, the situation of present reactions does not differ from most of the DI investigations, that is, no theoretical results are available. Two semi-empirical formulae have been developed (Fisher *et al* 1995, Bélenger *et al* 1997) for cross section predictions. Although these types of formulae do not explain the respective role of various individual DI processes, they are useful to determine the order of magnitude of total cross sections and to establish scaling laws. Present results are compared with the predictions of semi-empirical formulae and scaling laws. In particular, the scaling of data is analysed along the fluorine isoelectronic sequence by combining these results for O^- with those obtained for Ne^+ (Zambra *et al* 1994) and for Ar^{9+} (Zhang *et al* 1993). The high energy cross section behaviour is also investigated.

2. Method and apparatus

In this experiment, the animated crossed beams method (Defrance *et al* 1981) has been employed. The apparatus was essentially described earlier (Yu *et al* 1992). It was later equipped with a new ion beam production and transport system (Zambra *et al* 1994).

The experimental set-up is schematically shown in figure 1. The ion beam is extracted from a Colutron ion source in which carbon monoxide is introduced. The acceleration voltage is 4 kV. The extracted ion beam is focused by means of a pair of electrostatic lenses and mass

analysed by a 30°-magnet. The ion beam is collimated by a set of apertures into the collision region. The electron gun is the same as used in previous experiments. Ions are focused by a vertical electrostatic plane Einzell lens. In the subsequent 90° magnetic charge state analyser, product ions are deflected along an arc with a fixed radius of curvature to the detection system. A wide Faraday cup collects the primary ion beam. A spherical electrostatic deflector directs product ions to the channelplate detector.

The electron gun is schematically shown in the inset in figure 1. A ribbon-shaped electron beam is extracted from a Pierce-type cathode–anode configuration. The pair of plates acts simultaneously as a lens and as a beam deflector in the electron beam sweeping mode of the animated crossed beams method. The electron beam crosses the ion beam at a right angle inside the electrodes. The electrons are collected in a Faraday cup. Suppression plates provide total beam collection and prevent secondary electrons from interacting with the ion beam. A voltage can be applied to the wires in order to establish a potential barrier or a potential well to check the influence of residual ions trapped in the electron beam.

In the animated crossed beams method, the electron beam is swept across the ion beam in a linear see-saw motion at constant speed u which is measured by two thin wires located on both sides of the ion beam symmetrically, perpendicular to the electron beam trajectory.

3. Cross section measurement

The electron impact ionization cross section is related to the measured quantities in the following way (Defrance *et al* 1981):

$$\sigma = \frac{v_e v_i u K}{(v_e^2 + v_1^2)^{1/2}(I_e/e)(I_i/qe)}. \tag{1}$$

Here, u is the sweeping speed, K is the total number of events produced during one passage of electrons across the ion beam, v_e and v_i, I_e and I_i, e and qe are the velocities, currents and charges of the electrons and ions, respectively. In order to achieve good precision, careful measurements are needed for all the parameters in equation (1). The animated crossed beam method does not require the knowledge of beam density profiles.

The maximum electron energy is 2.5 keV. The electron energy is corrected for contact potentials and the kinetic energy of ions is taken into account to obtain the absolute collision energy. For the present experiment, a new type of cathode has been inserted in the electron gun and its support has also been changed. For this reason, the contact potentials have been carefully estimated by measuring the DI cross section for H^- around the threshold. The resulting contact potentials value is found to be 3.9 eV. According to previous experiments, electron energy spread (full width at half maximum (FWHM)) is estimated to be less than 1.7 eV.

The sweeping speed u is determined by measuring the time difference (t) between successive crossings of the electron beam over the wires, for a given amplitude V_1 of the sweeping ac voltage. During the measurements, this amplitude is reduced to a lower value V_2, so that the electron beam does not reach the wires. This procedure eliminates the production of secondary electrons by the wires. The scanning velocity is then given by the ratio:

$$u = \frac{dV_2}{tV_1}. \tag{2}$$

Here $d = 7.9$ mm is the distance between the wires.

The primary ion beam intensity is measured by the Faraday cup located inside the magnetic analyser. The magnetic field ensures total collection of ions and prevents secondary emission of electrons or ions, which would significantly affect the measurements. The available intensity

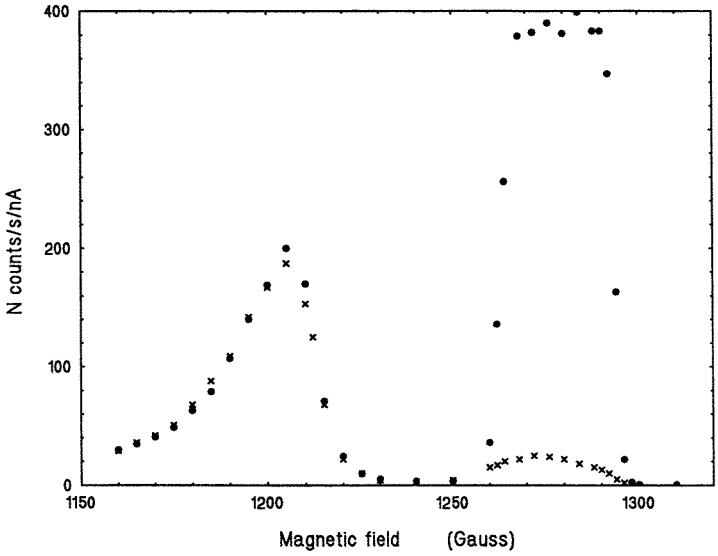

Figure 2. Count rate (O^+ from O^-) as a function of the analysing magnetic field with (●) and without (×) electron beam. The observation voltage is 300 V.

of beams is of the order of 0.4 nA for C^- and 5 nA for O^-. The primary ion current is integrated over the measurement time in order to eliminate errors due to the beam fluctuations. All apertures and slits between the collision region and both primary and product ion detectors are large enough to ensure essentially total ion transmission.

In this experiment, a positive voltage of 300 V is applied to the electrodes surrounding the interaction region so that the energy of positive ions formed inside this region is increased up to 4.6 keV. Ions formed outside this region do not undergo this kinetic displacement and are rejected by the magnetic analyser. During the measurements, the basic pressure in the collision region defined by application of this so-called observation voltage is kept below 10^{-9} mbar by means of appropriate pumps. The pressure outside this region is usually an order of magnitude higher. This procedure reduces the registered background by almost an order of magnitude. This is illustrated in figure 2 for oxygen: the count rate normalized with respect to the ion current is shown as a function of the analysing magnetic field with and without the presence of the electron beam. Positive ions having been formed inside the 300 V observation voltage are detected for an analysing magnetic field of 1279 G. The kinetic energy of positive ions formed outside this region remains almost identical to the initial negative ion acceleration energy so that these are detected around 1201 G. As a result, the background is reduced to about 5% of the total count rate only.

The detection efficiency was not measured directly. A pulse height distribution analysis has been performed in order to estimate the detectors effectiveness. From this procedure, a value of 0.61 ± 0.01 was attributed to the efficiency, which very closely corresponds to the ratio between the open area and the total area of the channelplates. The signal delivered by the detector is stored in a multichannel analyser in a multiscaling mode synchronously with the electron beam sweeping voltage. The usual form of the stored signal consists of two peaks, superimposed on the uniform background level. The peaks are accumulated during the passage of the electron beam upward and downward across the ion beam. The average of the background obtained outside of the peak regions is thus subtracted from the spectra and a net

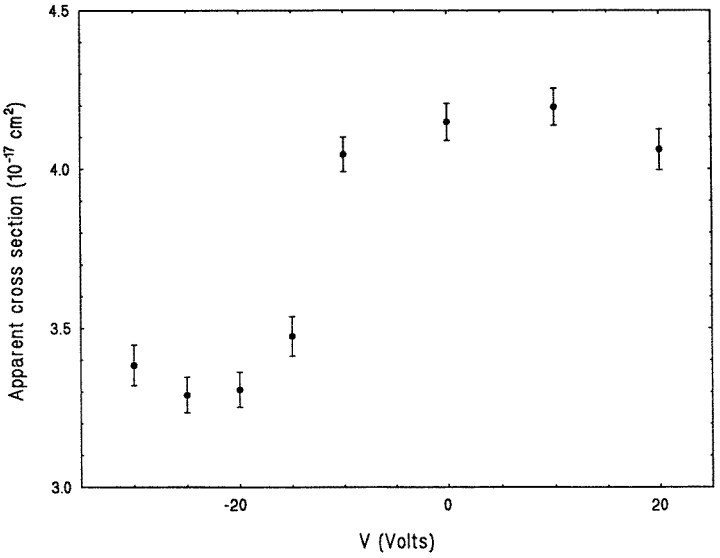

Figure 3. Apparent cross section for DI of C^- ($E_e = 300$ eV) as a function of the voltage applied to the wires (W), showing the influence of positive ions formed by electron impact.

signal for the cross section calculation is obtained.

The influence of slow positive ions formed by electron impact on residual gas has already been previously recognised (Defrance *et al* 1982). If these positive ions are trapped in the electron beam by the space–charge electric field, they contribute to the electron signal through the following reaction:

$$X^+ + Y^+ \rightarrow X^+ + \cdots . \tag{3}$$

In order to check for this contribution, apparent cross sections have been measured at 300 eV for different voltages applied to the wires. The results are shown in figure 3 for carbon. When passing from positive voltages (positive ions concentrated in the interaction region) to negative voltages (positive ions extracted from the interaction region), the apparent cross section drops by some 26% for C^- and by some 10% for O^-. Present results were obtained by applying a negative voltage (-25 V) to the wires, so that this effect is negligible.

Typical working conditions are listed in table 1. Estimated statistical and systematic uncertainties of measured quantities are also listed. Statistical uncertainty represents one standard deviation of the counting statistics. The total uncertainty, obtained in quadrature sum of uncertainties at the cross section maximum is found to be between 4.8% and 4.4% for C^- and O^-, respectively.

4. Results and discussion

The results are listed in tables 2 and 3 for C^- and O^- ions, respectively. Errors represent only one standard deviation of the counting statistics. For both ions the cross section is found to be zero below the respective first DI threshold within the corresponding absolute uncertainties. This indicates the absence of background modulation and of spurious contributions.

Figures 4 and 5 show, for C^- and O^-, respectively, the energy diagrams on which the data relevant for the present discussion are reported. These data are extracted from Hotop

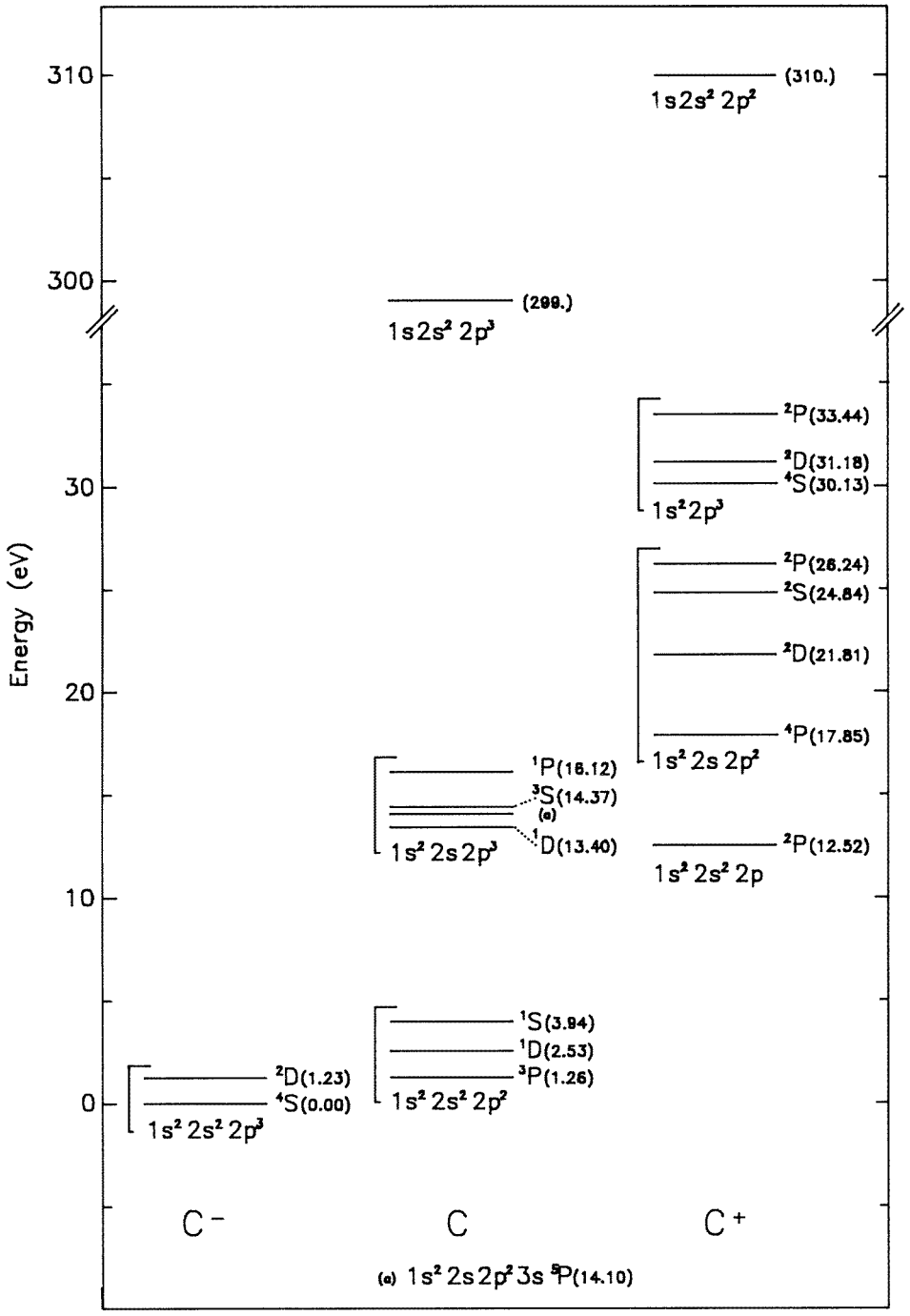

Figure 4. Diagram of energy levels for DI of C^-.

Table 1. Typical working conditions.

Parameter	Typical value	Error (%) systematic	Error (%) statistical
Kinematic factor $(v_e v_i q e^2 (v_e^2 + v_i^2)^{-1/2})$			
C^-	6.7×10^{-29}	0.5	—
O^-	5.8×10^{-29}	0.5	—
Sweeping speed (u)	4 m s^{-1}	1.0	1.0
Electron current (Ie)	0.1–1.5 mA	0.5	0.5
Detection efficiency (γ)	0.61	1.7	—
Ion current (I_i)			
C^-	0.4 nA	0.5	0.5
O^-	5.0 nA	0.5	0.5
Number of counts (K)			
C^-	0.02	—	2.0
O^-	0.18	—	0.4
Cross section (σ), (10^{-17} cm^2)			
C^-	8.2	4.2	2.3
O^-	5.4	4.2	1.3

and Lineberger (1985), Bashkin and Stoner (1975), Clementi and Roetti (1974), Caldwell and Krause (1993) and Saha (1994). The zero energy corresponds to the respective ground state of C^- and O^-, respectively. Results are also shown in figures 6 and 7 together with the experimental results of Steidl *et al* (1995) and with the results obtained by means of two semi-empirical formulae proposed by Fisher *et al* (1995) and by Bélenger *et al* (1997). The error bars represent the statistical uncertainty of the count rate K, only, as listed in the corresponding tables.

The different sets of experimental results are only in good agreement close to the ionization threshold. For C^-, present results are systematically lower than the others by some 25% around the maximum. For O^-, the maximum discrepancy is around 30% between 30 and 100 eV and reduces above this energy. An explanation of the observed discrepancies can be found in the procedure adopted in the Steidl experiment to eliminate the space–charge effects in the high intensity electron beam which are seen to influence the transmission of products ions from the collision region to the detector. In that experiment, argon gas is introduced in the collision chamber. Slow positive argon ions are formed by electron impact and trapped in the electron beam (see section 3). This results in the required space–charge neutralization but, as a consequence, negative ions may also interact with these slow positive ions (reaction (3)). The resulting spurious signal leads to cross sections which are overestimated by some 25% for C^- and 10% for O^-. This partially explains the observed discrepancies between the different experimental results. Moreover, this procedure strongly increases the background noise.

The comparison with the prediction of semi-empirical formulae (figures 6 and 7) show that, in the absence of any theoretical result, they give an estimation of cross sections which is within 50% of the experimental results. Unfortunately, both of the formulae fail to reproduce the details of the experimental results around the threshold as well as at high energy. In particular, the position of the cross section maximum is predicted to be slightly below the observed one.

The semi-empirical formulae include the scaling law proposed (Defrance and Yu 1992) to draw the overall evolution of the DDI cross section for atomic or ionic systems in which only

Table 2. DI of C^- by electron impact.

E_e (eV)	σ (10^{-17} cm^2)	$\Delta\sigma$ (10^{-17} cm^2)	E_e (eV)	σ (10^{-17} cm^2)	$\Delta\sigma$ (10^{-17} cm^2)
11.3	−0.11	0.13	146.3	5.92	0.13
13.3	0.12	0.24	171.3	5.29	0.11
14.3	0.11	0.16	196.3	4.86	0.10
15.3	0.29	0.11	221.3	4.34	0.09
16.3	0.38	0.12	246.3	3.95	0.08
17.3	0.71	0.11	266.3	3.79	0.04
18.3	0.88	0.09	276.3	3.70	0.07
19.3	1.06	0.11	286.3	3.56	0.04
20.3	1.19	0.12	296.3	3.39	0.02
21.3	1.42	0.12	301.3	3.31	0.03
22.3	1.66	0.11	306.3	3.30	0.04
23.8	2.13	0.13	308.3	3.37	0.04
26.3	2.55	0.15	311.3	3.30	0.04
28.8	3.01	0.14	313.3	3.24	0.04
31.3	3.57	0.14	316.3	3.12	0.04
33.8	4.32	0.14	321.3	3.09	0.04
36.3	4.81	0.14	326.3	3.09	0.04
41.3	5.99	0.17	336.3	2.97	0.04
46.3	6.92	0.18	346.3	2.95	0.05
51.3	7.42	0.16	371.3	2.66	0.05
56.3	7.77	0.14	401.3	2.59	0.04
61.3	8.17	0.12	501.3	2.06	0.04
66.3	8.15	0.12	601.3	1.69	0.04
71.3	7.91	0.09	701.3	1.47	0.03
76.3	7.54	0.09	796.3	1.38	0.06
78.3	7.54	0.14	896.3	1.19	0.05
81.3	7.84	0.13	996.3	1.13	0.05
86.3	7.73	0.11	1196.3	0.96	0.05
88.3	7.46	0.14	1396.3	0.80	0.05
91.3	7.35	0.13	1596.3	0.73	0.05
96.3	7.40	0.12	1796.3	0.73	0.05
106.3	6.94	0.13	1996.3	0.64	0.06
116.3	6.67	0.12	2246.3	0.56	0.07
131.3	6.23	0.15	2496.3	0.38	0.07

the L-shell is concerned. This scaling law gives the maximum of the cross section σ_m by:

$$\sigma_m = \frac{An_e(n_e - 1)}{2I^2} \tag{4}$$

where n_e is the number of electrons belonging to the shell, I the ionization potential and A is a fitting factor. The scaling of the C^- and O^- results with (4) clearly shows that this law does not apply here: σ_m largely reduces when passing from carbon to oxygen in spite of the two additional electrons present in the L-shell of the target. This conclusion is also immediately deduced from inspecting the large qualitative change of agreement between the experimental results and the prediction of the Fisher formula (figures 6 and 7).

Following Wannier (1955), various authors attempted to deduce the cross section energy dependence in the DDI threshold region. The result obtained for negative ions by Klar and Schlecht (1976) or by Grujic (1983) is:

$$\sigma \propto (E - I)^x \qquad \text{with} \quad x = 2.83. \tag{5}$$

Table 3. DI of O^- by electron impact.

E_e (eV)	σ (10^{-17} cm^2)	$\Delta\sigma$ (10^{-17} cm^2)	E_e (eV)	σ (10^{-17} cm^2)	$\Delta\sigma$ (10^{-17} cm^2)
12.3	0.01	0.04	196.3	4.75	0.03
15.3	0.03	0.03	221.3	4.60	0.02
16.3	0.01	0.01	246.3	4.26	0.01
17.3	0.03	0.01	271.3	3.99	0.02
18.3	0.08	0.02	296.3	3.71	0.01
19.3	0.13	0.02	346.3	3.40	0.02
20.3	0.17	0.02	396.3	3.11	0.02
21.3	0.26	0.01	446.3	2.82	0.02
22.3	0.31	0.02	496.3	2.57	0.01
23.3	0.36	0.03	516.3	2.52	0.02
24.3	0.44	0.02	536.3	2.43	0.02
25.3	0.54	0.02	546.3	2.40	0.02
26.3	0.64	0.02	556.3	2.36	0.01
28.3	0.84	0.01	561.3	2.35	0.01
30.3	0.98	0.02	564.3	2.36	0.01
32.3	1.24	0.02	566.3	2.39	0.01
34.3	1.44	0.03	568.3	2.39	0.01
36.3	1.71	0.03	571.3	2.34	0.01
41.3	2.20	0.04	576.3	2.33	0.01
46.3	2.86	0.05	581.3	2.32	0.02
56.3	3.84	0.03	586.3	2.30	0.02
61.3	4.17	0.05	591.3	2.31	0.02
66.3	4.58	0.03	596.3	2.29	0.01
71.3	4.64	0.05	616.3	2.26	0.02
76.3	4.74	0.04	636.3	2.16	0.01
81.3	4.99	0.05	656.3	2.14	0.01
86.3	5.04	0.04	676.3	2.11	0.01
91.3	5.19	0.05	686.3	2.06	0.02
96.3	5.23	0.04	696.3	2.02	0.01
101.3	5.25	0.04	746.3	1.94	0.02
103.3	5.43	0.05	796.3	1.82	0.01
106.3	5.43	0.02	896.3	1.64	0.01
111.3	5.43	0.03	996.3	1.53	0.02
113.3	5.40	0.03	1196.3	1.34	0.01
116.3	5.49	0.02	1396.3	1.14	0.02
118.3	5.43	0.04	1596.3	1.05	0.02
121.3	5.40	0.02	1796.3	0.94	0.01
126.3	5.43	0.02	1996.3	0.90	0.02
131.3	5.45	0.05	2196.3	0.83	0.02
136.3	5.39	0.02	2396.3	0.78	0.02
146.3	5.33	0.02	2596.3	0.68	0.02
171.3	5.11	0.02	—	—	—

From fitting present results, x is estimated to be 1.0 and 1.3 for C^- and O^-, respectively. These values show that the energy dependence is nearly linear, which evidently differs from the theoretical result. Furthermore, the experimental thresholds (C^-: 14.1 eV and O^-: 16.2 eV) are slightly higher than the lowest DDI expected thresholds (12.52 eV and 15.08 eV for C^- and O^-, respectively).

Among indirect ionization processes, IA frequently plays an important role in DI. In the

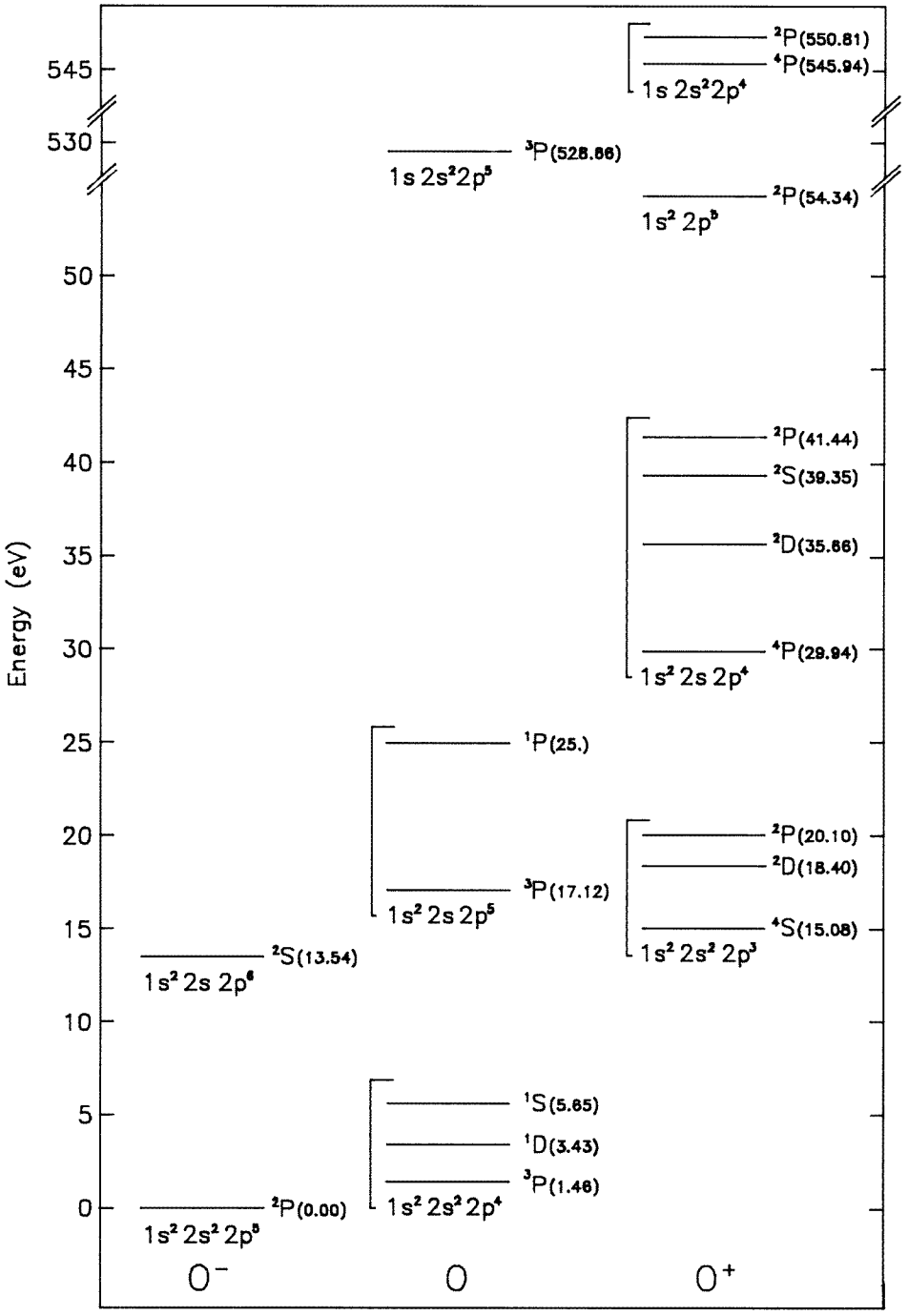

Figure 5. Diagram of energy levels for DI of O^-.

present cases, autoionizing states can be formed in the low energy region by ejection of one 2s-electron (figures 4 and 5). C and O atoms are left in the $1s^2 2s 2p^3$ and $1s^2 2s 2p^5$ configuration,

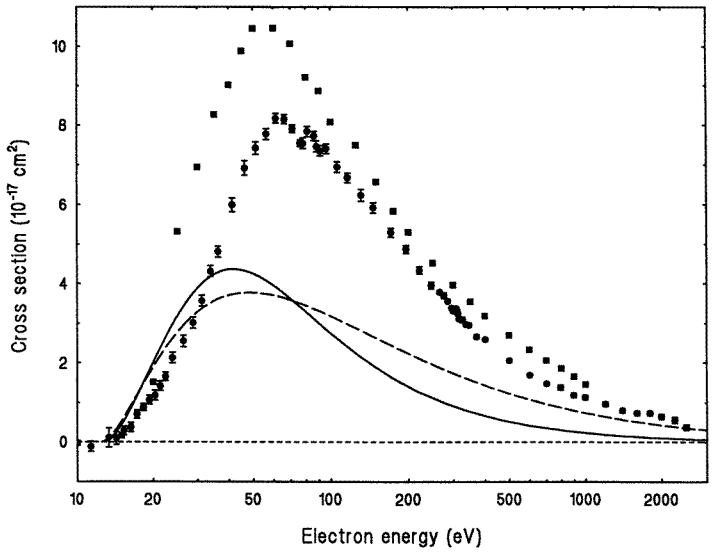

Figure 6. Absolute cross sections versus electron energy for electron impact DI of C^-: (●), present experimental results and (■) Steidl *et al* (1995). Error bars are only one standard deviation of statistical uncertainty. Curves are semi-empirical formulae predictions: (– – –), Bélenger *et al* (1997) and (—), Fisher *et al* (1995).

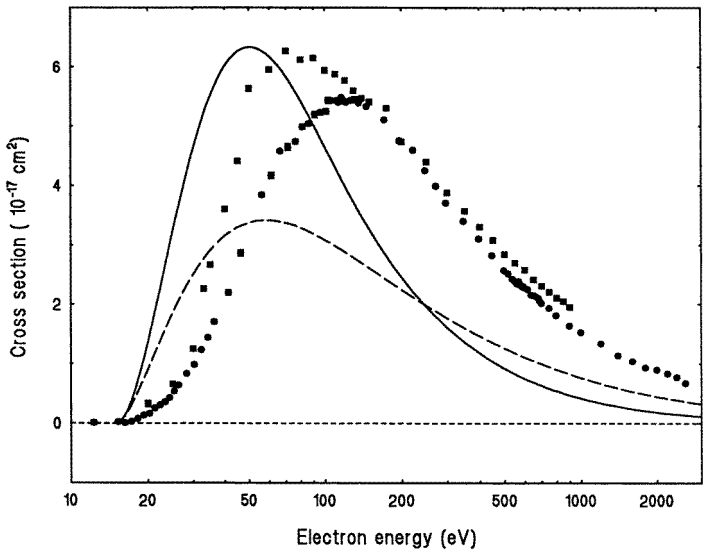

Figure 7. Absolute cross sections versus electron energy for electron impact DI of O^-, the same as figure 6.

respectively, whose singlet and triplet states are autoionizing. For C, these states are situated just above the DDI threshold (0.9–3.6 eV) so that it is not possible to distinguish their respective role from DI results. For O, ^{3}P and ^{1}P states can be formed at 2 eV and 10 eV above the DDI threshold, respectively. The lowest of them (^{3}P) is again too close to the threshold to be observed. The energy level of the ^{1}P state has been calculated by Baluja and Zeippen (1988),

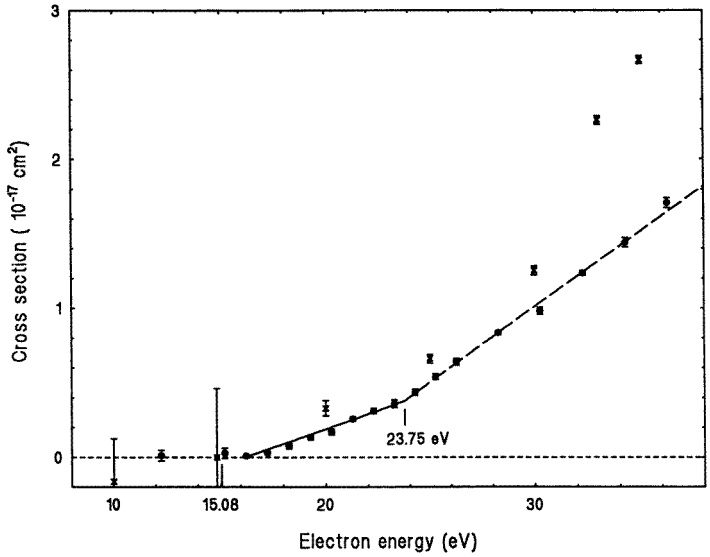

Figure 8. Cross section for electron impact DI of O^- in the low energy region, showing the IA threshold at 23.7 eV: (●), present results and (×), Steidel *et al* (1995).

but has so far never been observed. The present low energy data show a clear change of slope at 23.7 eV (figure 8). It is attributed to the opening of the IA process corresponding to the formation of the above-mentioned ^1P autoionizing state. There is nevertheless a disagreement of about 1 eV between the observed and the calculated values.

According to the Lotz semi-empirical formula (1967) applied in the high energy region, IA is expected to play a minor role above the K-shell ionization threshold only. Details of the results (figures 9 and 10) show weak, but significant irregularities both for C^- and O^-. Unfortunately, it is not possible to unambiguously attribute them to K-shell ionization.

The high energy behaviour of ionization cross sections in the Bethe–Born approximation is given by

$$\sigma = \frac{1}{EI}(a \ln E/I + b). \tag{6}$$

A Bethe-plot of data shows the leading asymptotic term. For single ionization (SI), the logarithmic term is usually dominant, while for DI, some experimental results show that the E^{-1} term (b) may be dominant. This latter case holds for H^-, for instance, where no indirect process can be present (Yu *et al* 1992). The Bethe plot of these results (figure 11) show a surprising difference between C^- and O^-: the C^- case is evidently dominated by the E^{-1} term but O^- is dominated by the logarithmic one, as for O^- detachment (Peart *et al* 1979). No direct argument can be found to explain such difference between these behaviours.

Direct SI cross sections are generally well reproduced by semi-empirical formulae which include the classical Thomson scaling law:

$$\sigma_m = \frac{B}{I^2}. \tag{7}$$

For DDI, semi-empirical formulae assume that this classical law is also valid, but this validity has never been checked along an isoelectronic sequence. The best check is obtained by plotting the product σI^2 against the energy in units of the ionization potential for various elements of an isoelectronic sequence. The fluorine sequence is analysed according to this

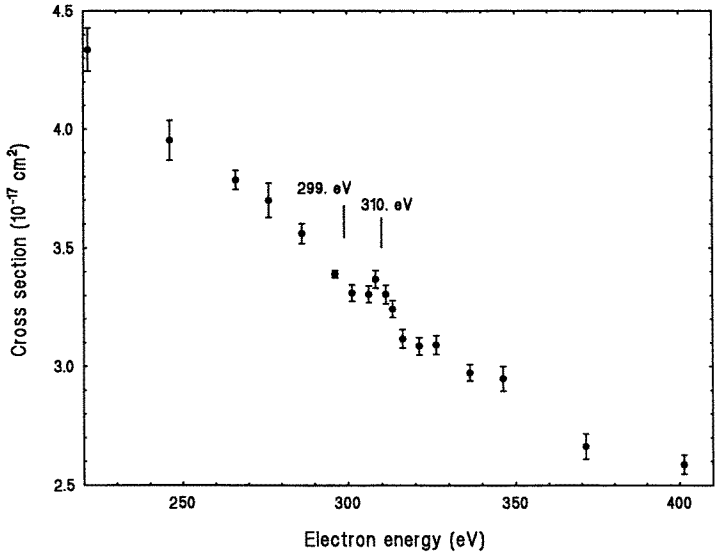

Figure 9. Absolute cross sections versus electron energy for electron impact DI of C^-, in the K-shell ionization threshold region. Thresholds for K-shell ionization (299 eV) and for (1s, 2p) DI (310 eV) are indicated.

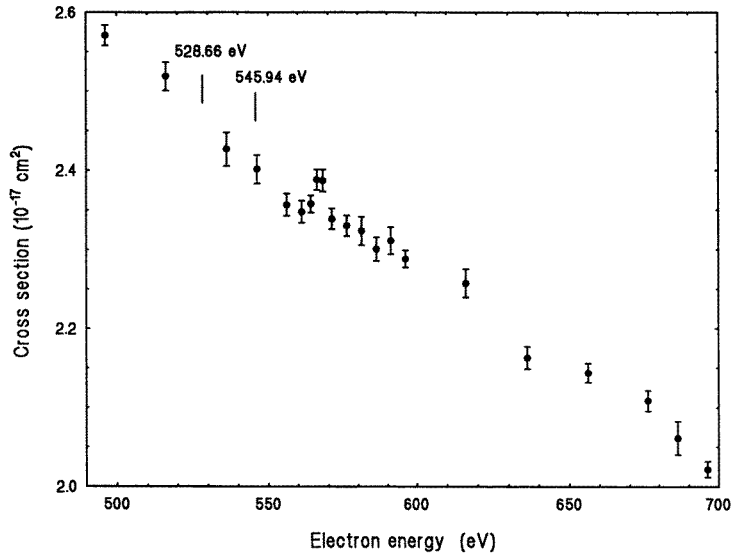

Figure 10. Absolute cross sections versus electron energy for electron impact DI of O^-, in the K-shell ionization threshold region. Thresholds for K-shell ionization (528.7 eV) and for (1s, 2p) DI (545.9 eV) are indicated.

procedure (figure 12) by combining the present O^- results with those obtained for Ne^+ (Zambra *et al* 1994) and Ar^{9+} (Zhang *et al* 1993). The Thomson scaling law is seen to be valid for weak charge states: the maximum is nearly identical for O^- and for Ne^+. For Ar^{9+}, this maximum is reduced by a factor of five. This results indicates that B strongly depends on the ion charge state within an isoelectronic sequence. A similar conclusion was obtained for the

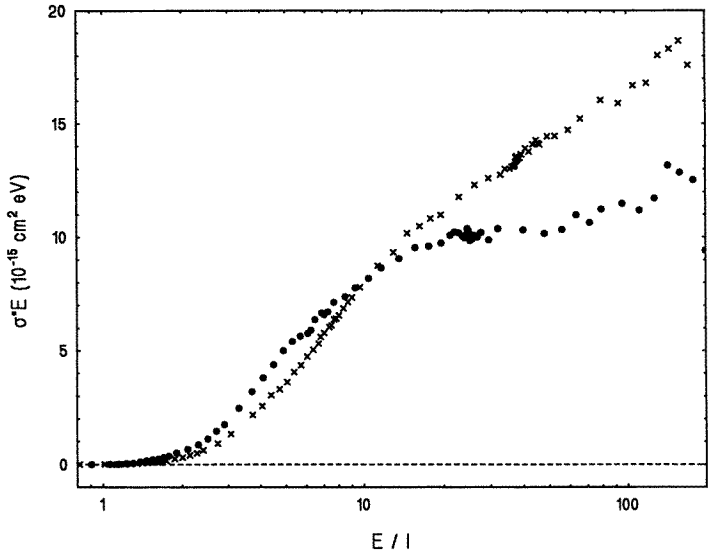

Figure 11. Bethe plot of absolute cross sections for electron impact DI of C^- (●) and O^- (×).

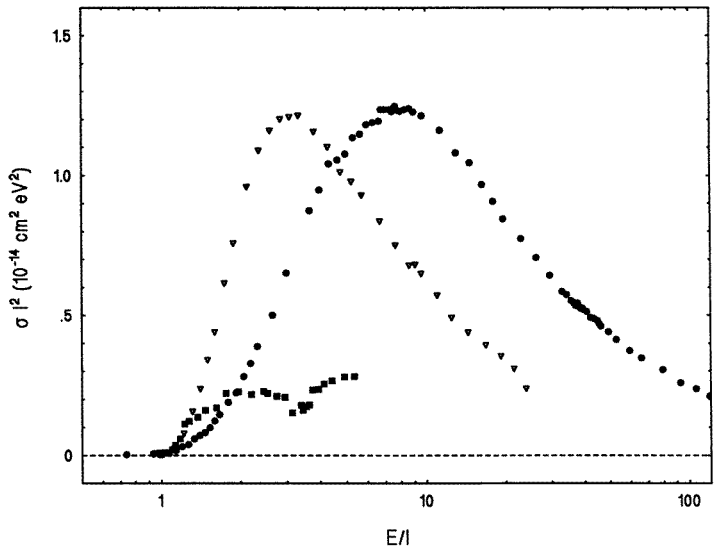

Figure 12. Scaled absolute cross sections (σI^2) for electron impact DI of O^- (●), Ne^+ (×) and Ar^{9+} (■) versus scaled electron energy (Ee/I).

beryllium sequence (C^+ and Ne^{5+}, Duponchelle *et al* 1997). Additional experimental data in the fluorine sequence should give more information about the charge state dependence of DDI cross section. This fact certainly results from the dominant role of correlation between target electrons. Theoretical developments and calculations should give a description of this effect.

It is worthwhile to note the significant threshold energy shift (see above) which was also observed for other ions. For Ne^+, cross section measurements have been repeated with this apparatus in the threshold region. From these measurements, the DDI threshold was given a

value of 110.6 eV, that is, 5.2 eV above the published value (Bashkin and Stoner 1975). For Ar^{9+}, a shift of the order of 80 eV was observed. This shift could indicate that the residual ion is left in an excited state or that the observed DDI thresholds correspond to ejection of two electrons belonging to two different sub-shells.

For O^-, the cross section maximum is reached at about eight times the ionization potential, which differs strongly from the most frequently encountered situation and which holds for Ne^+ and Ar^{9+} (about three times the ionization potential). The large bump shown for Ar^{9+} above 3.5 corresponds to the K-shell IA. This process is roughly reproduced by the predictions of the Lotz (1968) semi-empirical formula.

5. Summary

Absolute cross section measurements are reported for DI of C^- and O^- ions by electron impact. The presence of slow positive ion trapping in the electron beam explains the discrepancy between these results and those of Steidl *et al* (1995). In the absence of any theoretical results, semi-empirical formulae roughly reproduce the experimental results but not the details of them. In addition, the scaled results deviate strongly from the classical Thomson law for multiply charged ions in the fluorine isoelectronic sequence.

The autoionizing ^1P state belonging to the $1s^22s2p^5$ oxygen configuration has been observed for the first time and its experimental energy level determined to be 23.7 eV with respect to the O^- ground state level. There is also experimental evidence of the role of autoionizing states around the K-shell ionization threshold. Several features have been observed, regarding the threshold energy shift, the position of the cross section maximum and the asymptotic energy dependence. Unfortunately, no theoretical calculation or argument is able to give a rough explanation of these observations.

Acknowledgment

The authors are grateful to Professor E Salzborn for providing us with unpublished results.

References

Baluja K and Zeippen C J 1988 *J. Phys. B: At. Mol. Phys.* **21** 15
Bashkin S and Stoner J O 1975 *Atomic Energy levels and Grotrian Diagrams* (Amsterdam: North-Holland)
Bélenger C, Defrance P, Salzborn E, Shevelko V P, Uskov D B and Tawara H 1997 *J. Phys. B: At. Mol. Opt. Phys.* **30** 729
Caldwell C D and Krause M O 1993 *Phys. Rev.* A **47** R759
Clementi E and Roetti C 1974 *At. Data Nucl. Data Tables* **14** 177
Defrance P, Brouillard F, Claeys W and Van Wassenhove G 1981 *J. Phys. B: At. Mol. Phys.* **14** 103
Defrance P, Claeys W and Brouillard F 1982 *J. Phys. B: At. Mol. Phys.* **15** 3509
Defrance P and Yu D J 1992 *Proc. 17th Int. Conf. Physics of Electronic and Atomic Collisions (Brisbane)* (Bristol: Hilger) p 323
Defrance P, Yu D J and Belic D S 1993 *Proc. 18th Int. Conf. Physics of Electronic and Atomic Collisions (Aarhus)* ed T Andersen *et al* p 370
Fisher V, Ralchenko Y, Goldgirsh A, Fisher D and Maron Y 1995 *J. Phys. B: At. Mol. Opt. Phys.* **28** 3027
Grujic P 1983 *J. Phys. B: At. Mol. Phys.* **16** 2567
Hotop H and Lineberger W C 1985 *J. Phys. Chem. Ref. Data* **14** 731
Klar H and Schlecht W 1976 *J. Phys. B: At. Mol. Phys.* **10** 1699
Lotz W 1967 *Z. Phys.* **206** 205
Moores D L and Reed K J 1994 *Adv. At. Mol. Opt. Phys.* **34** 301
Peart B, Forrest R A and Dolder K 1979 *J. Phys. B: At. Mol. Phys.* **12** 847
——1979 *J. Phys. B: At. Mol. Phys.* **12** 2735

Saha H P 1994 *Phys. Rev.* A **49** 894
Steidl M 1994 Doppelionisation von C^-, O^- und F^--Ionen durch elektronenstoss *Diplomarbeit*, University of Giessen, Germany
Steidl M, Hathiramani D, Hofmann G, Stenke M, Völpel R and Salzborn E 1995 *Proc. 19th Int. Conf. Physics of Electronic and Atomic Collisions (Whistler)* ed J B A Mitchell *et al* p 564
Yu D J, Rachafi S, Jureta J and Defrance P 1992 *J. Phys. B: At. Mol. Opt. Phys.* **25** 4593
Wannier G H 1955 *Phys. Rev.* **100** 1180
Zambra M, Belic D, Defrance P and Yu D J 1994 *J. Phys. B: At. Mol. Opt. Phys.* **27** 2383
Zhang H, Duponchelle M, Bélenger C, Oualim EM and Defrance P 1993 *Proc. 18th Int. Conf. Physics of Electronic and Atomic Collisions (Aarhus)* ed T Andersen *et al* p 369